Dynamic electrochemical impedance spectroscopy of quasi-reversible redox systems. Properties of the Faradaic impedance, and relations to those of voltammograms

Tamás Pajkossy

Institute of Materials and Environmental Chemistry

Research Centre for Natural Sciences, Hungarian Academy of Sciences

Magyar tudósok körútja 2, Budapest, Hungary, H-1117

e-mail: pajkossy.tamas@ttk.mta.hu

Abstract

By analysing the electrochemical impedance spectra (EIS) of quasi-reversible redox systems, the two elements of the Faradaic impedance: charge transfer resistance and the coupled Warburg-coefficient can be obtained at a given potential. The same applies also to DEIS (dynamic EIS) measurements, when high frequency impedance spectra are measured while the potential is scanned to simultaneously accomplish cyclic voltammetry or other transient measurements. In case of DEIS both the charge transfer resistance and the Warburg coefficient depend on the applied potential program, e.g. on scan-rate. A theory is presented, yielding a transformation by which this dependence can be eliminated. The proposed procedure yields two, scan-rate independent, hysteresis-free functions, which are closely related to the EIS results, and also to the functions which are the transformed forms of the cyclic voltammograms as suggested in T. Pajkossy, S. Vesztergom, *Electrochim. Acta,* **297** (2019) 1121. To illustrate the properties of the transformations and the functions involved, numerical simulations are also presented. The theory opens a new route for the high-accuracy, fast determination of charge transfer rate coefficients of quasi-reversible redox systems by employing DEIS.

1. Introduction

Electrochemical impedance spectroscopy (EIS) is a measurement method that requires the equilibrium, or at least steady state, of the studied electrochemical system. In practice, slowly changing systems can often be regarded quasi-stationary for sufficiently fast EIS measurements. This way repetitive EIS measurements can serve as a characterization method of the system's temporal evolution; such sequencing of EIS measurements is called dynamic EIS, DEIS. The fast impedance spectrum measurement is achieved by the use of multifrequency (rather than with stepped single frequency) perturbations; a number of spectra can be recorded in a couple of seconds, e.g. during one or a few cycles of a cyclic voltammogram, CV.

The history of DEIS can be traced back to the use of fast Fourier transform (FFT) used for AC polarography by Smith in the seventies [1]. Since then a number of devices have been constructed for the purpose of DEIS and various electrochemical phenomena were studied either by DEIS or by equivalent methods of different names [2,3,4,5,6,7,8].

Although DEIS is a useful method of characterizing electrochemical systems, DEIS spectra are not necessarily the same as those measured with traditional EIS, in which case the system can be considered more stationary. In this paper we analyse the difference of DEIS and EIS spectra based on an archetype reaction of electrode kinetics, diffusion controlled charge transfer. In the theory of voltammetry, these systems are often referred to as quasi-reversible redox systems and their properties belong to the core of the electrochemistry textbooks [9].

In the theory of EIS, quasi reversible redox systems are typically represented by the Randles-circuit; the Faradaic impedance therein is a serial combination of the charge transfer resistance and of the Warburg impedance (i.e. the diffusional impedance in case of planar electrodes); for the properties see [10]. In traditional EIS, these two quantities depend on the electrode potential E; in the case of DEIS measurements, however, an additional implicit dependence on time appears. As a result, DEIS spectra depend on the applied potential program, above all on the scan-rate.

The analysis of the DEIS spectra of quasi-reversible redox systems have been attempted in a couple of previous papers [4,5,6,7] – these, however, led to complicated results. The theory of the present paper, in contrast, leads to a simple procedure – to an extrapolation – by which scan-rate dependences can be eliminated. It yields two scan-rate independent, hysteresis-free, potential program invariant (PPI) functions, which are closely related to the EIS results, and to the functions which are the transformed forms of the CVs as suggested in a previous related paper [11].

2

The properties of the transformations and the functions involved are illustrated by numerical simulations.

2. Theory

Consider a quasi-reversible redox system with the condition that both the reduced and oxidized forms are present. These species take part in an *n*-electron charge transfer reaction with no detectable intermediates on a planar electrode. The general kinetic equation for this system describes the time dependence of the current density:

$$j(t) = n\mathrm{F}\big[k_{\mathrm{a}}\big(E(t)\big)\, c_{\mathrm{red}}^{\mathrm{s}}(t) - k_{\mathrm{c}}\big(E(t)\big)\, c_{\mathrm{ox}}^{\mathrm{s}}(t)\big] \qquad (1)$$

where the concentrations are surface ones (see the superscript "s"); the subscripts red and ox refer to reduced and oxidized species, respectively; F is the Faraday-constant. The dependence of the k_{a} anodic and k_{c} cathodic rate coefficients on electrode potential *E* does not have to be specified; all what is assumed is that they lie in a range to make both the anodic and cathodic reactions partially diffusion controlled. All potential dependencies of the quantities in the equations below can be traced back to that of the rate coefficients. The surface concentrations depend explicitly solely on time: this is due to the hindered diffusion of the redox species. With no hindrance, i.e. in the case of infinite tansport rate, Eq.(1) can be simplified to an equation where the concentrations are bulk ones:

$$j_{\mathrm{inf}}(E) = n\mathrm{F}[k_{\mathrm{a}}(E)c_{\mathrm{red}} - k_{\mathrm{c}}(E)c_{\mathrm{ox}}] \qquad (2)$$

We apply the usual assumptions that the redox species are minority components of the electrolyte and that any effects due to double layer charging, electrolyte resistance, migration and convection can be disregarded.

The expressions of the Faradaic impedance of this system – since the work of Randles in 1947 [12] – have appeared in many and diverse versions in textbooks and monographs, e.g. in Section 4.2 of [13] or Section 10 of [9]. We will adhere to the early theory of de Levie and coworkers [14,15] mostly because of two reasons: first, there has been made no *a priori* assumption on the actual dependence of rate coefficients on potential, and second, Ref. [15] is a study where the strong coupling of the charge transfer resistance, R_{ct}, and the Warburg coefficient, σ_{W}, has been emphasized. This coupling plays an important role also in the present theory. For a given potential *E,* the following equations were obtained:

Eq.6 of [15] reads as

$$\frac{1}{R_{ct}} = n\text{F} \left(\bar{c}_{red}^s \frac{dk_a}{dE} - \bar{c}_{ox}^s \frac{dk_c}{dE} \right)$$ (3)

where – just as in Eq.(1) – the c^s concentrations are surface ones, but the overlining means that these are mean (time-averaged) quantities, i.e. their periodic perturbations caused by the impedance measurement are already eliminated.

Eqs. 3 and 9 of Ref. [15] give the following equation for the Warburg impedance:

$$Z_W = \frac{\sigma_W^I(1 - \text{i})}{\sqrt{\omega}} = \frac{\sigma_W}{\sqrt{\text{i}\omega}} = \frac{k_a/\sqrt{D_{red}} + k_c/\sqrt{D_{ox}}}{\sqrt{\text{i}\omega}} \cdot R_{ct}$$ (4)

where D_{red} and D_{ox} denote the diffusion coefficients of the reduced and the oxidized species, respectively, i is the imaginary unit and ω is angular frequency. Note the difference of the two σ_W parameters: σ_W^I is the Warburg parameter that appears in related theories and that is recommended by IUPAC [10]. Instead of σ_W^I, in what follows we prefer the use of the $\sigma_W = \sigma_W^I/\sqrt{2}$ quantity, because it yields more compact formulae. It is expedient at this point to define the quantity H as

$$H = \sigma_W / R_{ct} = k_a/\sqrt{D_{red}} + k_c/\sqrt{D_{ox}}$$ (5)

Eqs. (3) to (5) have two important features. First, at a given potential σ_W and R_{ct} are proportional to each other; the proportionality constant contains neither bulk nor surface concentrations but only process rate coefficients, as a parameter combination (the intriguing consequences of the coupling are demonstrated in Ref. [15]). Second, in the equations of the Faraday impedance the surface concentrations (rather than bulk ones) appear. In traditional EIS measurements – that is, taking spectra after a sufficiently long initial delays – the net current is zero, the surface concentrations are determined by the Nernst equation; hence R_{ct} and σ_W are unique functions of potential.

Here the question appears: what if the net current is not zero, and surface concentrations are slowly changing due to a potential scan – i.e. when DEIS experiment is performed. In this case, Eqs. (3)-(5) would still hold, but σ_W and R_{ct} will depend on the electrode potential not only due to the potential dependencies of the rate coefficients, but also due to the inherent time dependence of the surface concentration changes. This is expressed by the Matsuda-Ayabe equations [16] as follows:

$$c_{red}^{s}(t) = c_{red} - \frac{1}{nF\sqrt{D_{red}}} \cdot M(t) \tag{6}$$

and

$$c_{ox}^{s}(t) = c_{ox} + \frac{1}{nF\sqrt{D_{ox}}} \cdot M(t) \tag{7}$$

Here the $M(t)$ function is a convolution, with u as a convolution variable,

$$M(t) = \frac{1}{\sqrt{\pi}} \int_0^t \frac{j(u)}{\sqrt{t-u}} du \tag{8}$$

This function has been named by Oldham [17,18] as „semiintegrated current". Note that for other than planar electrode geometries Eq.(8) is to be modified; this is, however, beyond our present scope.

For analysing DEIS situations, we have to introduce the surface concentrations (Eqs (6) and (7)) into Eq. (3) by calculating the convolution M up till the time of reaching the potential E. In what follows, $M(t(E)$ will be simply denoted as M; the combination yields

$$\frac{1}{R_{ct}} = nF\left(\bar{c}_{red}^{s}\frac{dk_a}{dE} - \bar{c}_{ox}^{s}\frac{dk_c}{dE}\right) = nF\left(\left(c_{red} - \frac{M}{nF\sqrt{D_{red}}}\right)\frac{dk_a}{dE} - \left(c_{ox} + \frac{M}{nF\sqrt{D_{ox}}}\right)\frac{dk_c}{dE}\right)$$

$$= nF\left(c_{red}\frac{dk_a}{dE} - c_{ox}\frac{dk_c}{dE}\right) - nF\left(\frac{1}{\sqrt{D_{red}}}\frac{dk_a}{dE} + \frac{1}{\sqrt{D_{ox}}}\frac{dk_c}{dE}\right) \cdot M \tag{9}$$

In Eq (9) the coefficient of M is the potential derivative of H, defined by Eq.(5). The first term equals the potential derivative of the current density j_{inf} that could be measured in the absence of any diffusional hindrance (i.e., when surface and bulk concentrations are equal). At this point we introduce the quantity $R_{ct,inf}$ as

$$\frac{1}{R_{ct,inf}} = \frac{dj_{inf}}{dE} = nF\left(c_{red}\frac{dk_a}{dE} - c_{ox}\frac{dk_c}{dE}\right) \tag{10}$$

which allows the simplification of Eq. (9)to

$$\frac{1}{R_{ct}} = \frac{1}{R_{ct,inf}} - \frac{dH}{dE} \cdot M \tag{11}$$

Since σ_W and R_{ct} are coupled to each other (cf. Eq. (5)), we get a similar equation for σ_W:

5

$$\frac{1}{\sigma_W} = \frac{1}{H} \cdot \left(\frac{1}{R_{ct,inf}} - \frac{dH}{dE} \cdot M \right) = \frac{1}{H \cdot R_{ct,inf}} - \frac{1}{H} \cdot \frac{dH}{dE} M \tag{12}$$

Further equations are available to connect impedance and CV-related quantities. This is based on a recent theory [11] on the PPI form of CVs (or of voltammograms of arbitrary $E(t)$ potential programs) of quasi-reversible redox systems. Accordingly, if a voltammogram is taken (or a set of voltammograms is taken) with the initial condition that no concentration gradients exist before time zero (accordingly, $j(t \le 0) = 0$) then, for the js and the Ms at identical potentials E the

$$j = j_{inf} - H \cdot M \tag{13}$$

and the

$$M = M_{rev} - 1/H \cdot j \tag{14}$$

equtions hold. From Eqs. (13) and (14) follows that

$$H = j_{inf}/M_{rev} \tag{15}$$

The physical meaning of M_{rev} is the semiintegral of the CV of a reversible system. By the above equations one can transform voltammograms to a form as if no diffusion hindrance were present (to j_{inf}, cf. Eq. (13)) or if the charge transfer were completely diffusionally controlled (to M_{rev}, cf. Eq. (14)). Parameter H (cf. Eq. (15)) has just the same physical meaning as in Eq. (5), $H = k_a/\sqrt{D_{red}} + k_c/\sqrt{D_{ox}}$.

By the combination of Eqs (11) and (14) we get

$$\frac{1}{R_{ct}} = \frac{1}{R_{ct,inf}} - \frac{dH}{dE} \cdot M = \frac{dj_{inf}}{dE} - \frac{dH}{dE} \cdot \left(M_{rev} - \frac{j}{H} \right) =$$

$$= \frac{d(H \cdot M_{rev})}{dE} - \frac{dH}{dE} \cdot M_{rev} + \frac{1}{H} \frac{dH}{dE} \cdot j = H \cdot \frac{dM_{rev}}{dE} + \frac{1}{H} \frac{dH}{dE} \cdot j \tag{16}$$

By combining Eqs. (12) and (14) we get

$$\frac{1}{\sigma_W} = \frac{1}{H} \left(\frac{1}{R_{ct,inf}} - \frac{dH}{dE} \cdot M \right) = \frac{1}{H} \frac{dj_{inf}}{dE} - \frac{1}{H} \frac{dH}{dE} \left(M_{rev} - \frac{j}{H} \right) =$$

$$= \frac{1}{H} \left(\frac{d(H \cdot M_{rev})}{dE} - \frac{dH}{dE} \cdot M_{rev} \right) + \frac{1}{H^2} \frac{dH}{dE} \cdot j = \frac{dM_{rev}}{dE} + \frac{1}{H^2} \frac{dH}{dE} \cdot j \tag{17}$$

To resume, all four equations (Eqs. (11),(12),(16),(17) express linear relations, from their intercepts and slopes the potential derivatives of j_{inf}, M_{rev} and H – all of which are PPI functions – can be

6

obtained. This is summarized in the following table, which contains also the linear equations of the CV case, Eqs (13) and (14):

Eq.No.	dependence	intercept	slope
(13)	j vs M	j_{inf}	$-H$
(14)	M vs j	M_{rev}	$-1/H$
(11)	$1/R_{\text{ct}}$ vs M	$\text{d}j_{\text{inf}}/\text{d}E$	$-\text{d}H/\text{d}E$
(12)	$1/\sigma_{\text{W}}$ vs M	$(1/H) \cdot \text{d}j_{\text{inf}}/\text{d}E$	$-(1/H) \cdot \text{d}H/\text{d}E$
(16)	$1/R_{\text{ct}}$ vs j	$H \cdot \text{d}M_{\text{rev}}/\text{d}E$	$+(1/H) \cdot \text{d}H/\text{d}E$
(17)	$1/\sigma_{\text{W}}$ vs j	$\text{d}M_{\text{rev}}/\text{d}E$	$+(1/H^2) \cdot \text{d}H/\text{d}E$

Table 1. The linear dependences.

3. Discussion

3.1. Limiting cases

There are two limiting cases worth to be tested:

(i) At very short times following the start of scanning or polarization ($t \sim 0$), or at very high scan-rates (when there is little if any diffusion hindrance), the surface concentrations remain the same as prior to scanning; that is, the same as in the bulk. Hence $j(E) = j_{\text{inf}}(E)$ and $M(t) \cong 0$. Thus the intercept of the $1/R_{\text{ct}}$ vs $M(t)$ line (cf. Eq. (11)) is $1/R_{\text{ct,inf}}$, i.e. the slope of the diffusion-free polarization curve.

(ii) At very long times ($t \rightarrow \infty$) or at very low (effectively zero) scan-rates, the surface concentrations reach a steady state and they are determined by the actual potential and the Nernst equation. (This is the "dc reversible case", which has been analysed e.g. in Ch.4.2.2 of Ref. 13.) Within the framework of the present kinetics-centered analysis, this means that $k_{\text{a}}(E)c_{\text{red}}^{\text{s}} = k_{\text{c}}(E)c_{\text{ox}}^{\text{s}}$, cf. Eq. (1). In this case $j=0$, hence the intercept of the $1/\sigma_{\text{W}}$ vs $j(t)$ line is $\text{d}M_{\text{rev}}/\text{d}E$ (cf. Eq.18). This property has already been shown, in a more general form, in [19].

Eqs.(16) and (17) allow us to define

$$R_{\text{ct,ss}} = R_{\text{ct}}(t \rightarrow \infty) = 1/(H \cdot \text{d}M_{\text{rev}}/\text{d}E) \tag{18}$$

and

$$\sigma_{\text{W,ss}} = \sigma_{\text{W}}(t \rightarrow \infty) = 1/(\text{d}M_{\text{rev}}/\text{d}E) \tag{19}$$

where ss in the subscript refers to steady state. These are the quantities which are obtained from EIS measurements.

3.2. Tests of typical cases: numerical simulations (I)

To illustrate the properties of the functions and transformations involved in the previous section, a set of CVs, $R_{ct}(E)$, and $\sigma_W(E)$ functions have been simulated numerically. The calculations of the PPI functions were carried out from these functions afterwards. The input functions of the simulation are the $H(E)$, $j_{inf}(E)$ functions; from these the $M_{rev}(E) = j_{inf}(E)/H(E)$ and the derivatives dH/dE, dj_{inf}/dE, and dM_{rev}/dE have also been calculated. These functions are shown in Fig.1, with the electrochemistry-related parameters of the simulations listed in the legend.
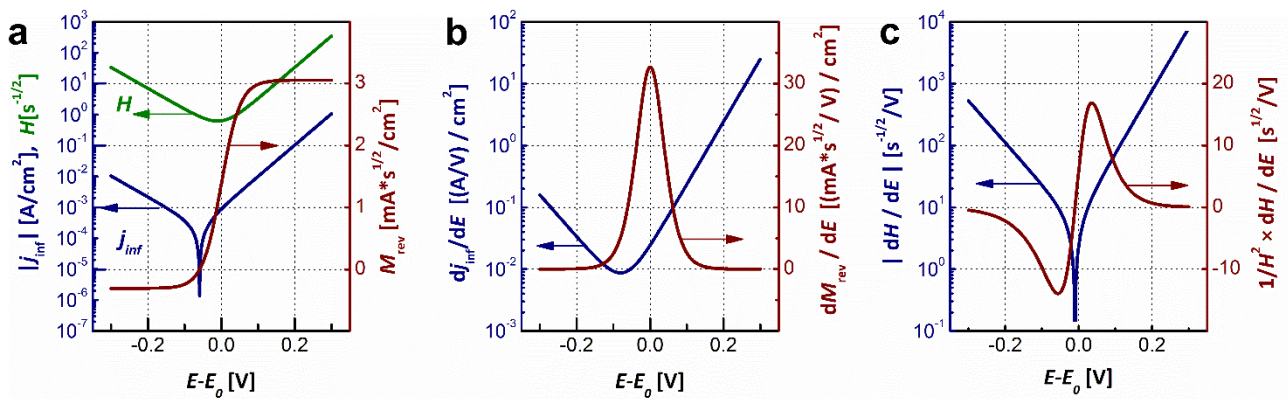
Fig.1. PPI input functions of the simulations (a) and related derived functions (b) and (c). The electrochemistry-related parameters of the simulation are as follows: $c_{red}^b = 10^{-5}\mathrm{mol/cm^3}$, $c_{ox}^b = 10^{-6}\mathrm{mol/cm^3}$, $D_{red} = D_{ox} = 10^{-5}\mathrm{cm^2/s}$; $k_a(E) = k_0\exp(\alpha_a F(E - E_0)/RT)$ and $k_c(E) = k_0\exp(-\alpha_c F(E - E_0)/RT)$ with $k_0 = 10^{-3}\mathrm{cm/s}$; $\alpha_a = 0.6$ .and $\alpha_c = 0.4$.

The simulations were performed in a novel way: In contrast to the simulations in Ref [11], where the CVs were calculated with a traditional explicit Euler method of solving the diffusional equation [20], here we applied the fast semiintegration algorithm of Ref. [21], thereby employing a new, fast method to calculate the $j(t)$ and $M(t)$ functions and hence the $1/R_{ct}(t)$ and $1/\sigma_W(t)$ curves as well for the quasi-reversible redox systems. The simulation procedure is shown as a pseudocode in Appendix A.

The potential program starts at the actual redox potential, i.e. at E_0-0.059 V, then one complete cycle is performed with E_0+0.3V and E_0-0.3V potential limits with scan-rates as indicated on the

8

plots. The effects of IR drop and double-layer charging are disregarded; the time resolution of the simulation is 0.1ms; the potential resolution is 1mV (all data points were averaged in 1mV potential intervals).

The simulated $j(E(t))$, $M(E(t))$ functions and the reciprocals of the $R_{ct}(E(t))$ and $\sigma_W(E(t))$ functions are shown in Fig.2. These four are the input data for the subsequent calculations, which comprise two steps:

First, linearity of the $1/R_{ct}$ vs M and of the $1/\sigma_W$ vs j functions (cf. Eqs. (11) and (17)) is demonstrated in Figs 3a and 3b.

Second, the ordinate intercepts and the slopes of these lines are calculated using a linear least squares fitting procedure [22] and are plotted as a function of potential. The ordinate intercepts of the $1/R_{ct}$ vs M lines ($=1/R_{ct,inf} = dj_{inf}/dE$, cf. Eq.(11)) are shown in Fig.3c as blue diamonds. These points lie on the top of the solid line of the input function dj_{inf}/dE (same as the one in Fig.1b). The intercepts of the $1/\sigma_W$ vs j lines, ($=1/\sigma_{W,ss} = dM_{rev}/dE$, cf. Eq. (17))), plotted in Fig.3d as blue diamonds, fitting well to the solid line of dM_{rev}/dE, which is another input function, same as the one in Fig.1b.

The slopes of the $1/R_{ct}$ vs M lines, ($=dH/dE$, cf. Eq.(11)) are plotted in Fig.3c as red circles. These points lie on the top of the solid line of the input function dH/dE (same as the one in Fig.1c). Finally, for the sake of completeness, the slopes of the $1/\sigma_W$ vs j lines, ($= (1/H^2) \cdot dH/dE$, Eq. (17)) are plotted in Fig.3d as blue diamonds. Theses points fit well to the solid line of $(1/H^2) \cdot dH/dE$ which is calculated from the input function, same as the one in Fig.1c.

Note that in each four case of Figs 3c and 3d the plots of the symbols lie on (or very close to) the solid lines, indicating that using the extrapolation procedure we obtain the same data as those of the input functions. The self-consistency of the simulation+extrapolation procedure is supported by the lack of hysteresis on the $1/R_{ct,inf}(E)$ and the $1/\sigma_{W,ss}(E)$ curves.
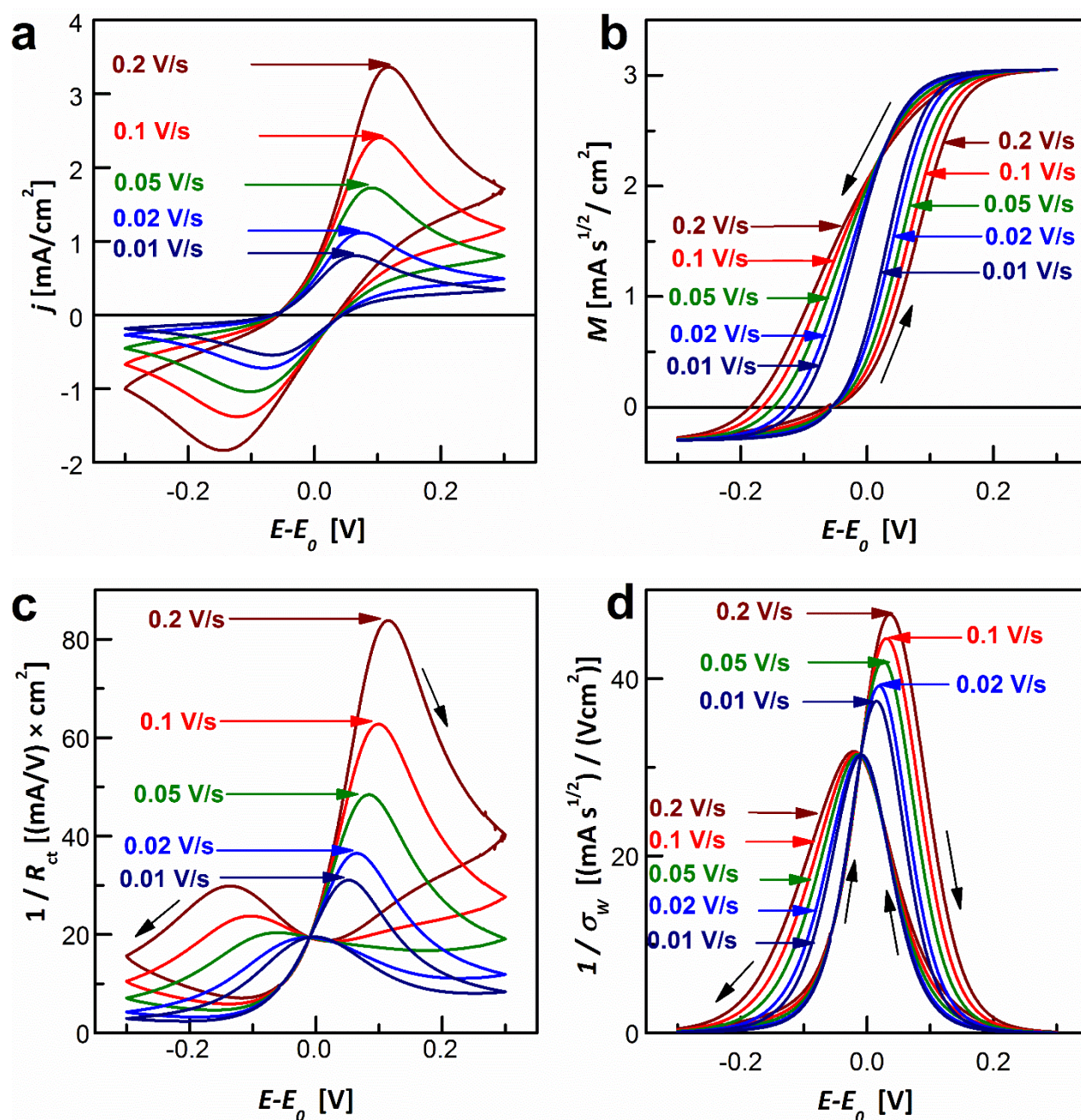
Fig.2. Simulated curves at scan-rates as indicated. **a.)** The CVs. **b.)** The semiintegrated CVs. **c.)** The $1/R_{ct}(E)$ functions. **d.)** The $1/\sigma_W(E)$ functions.
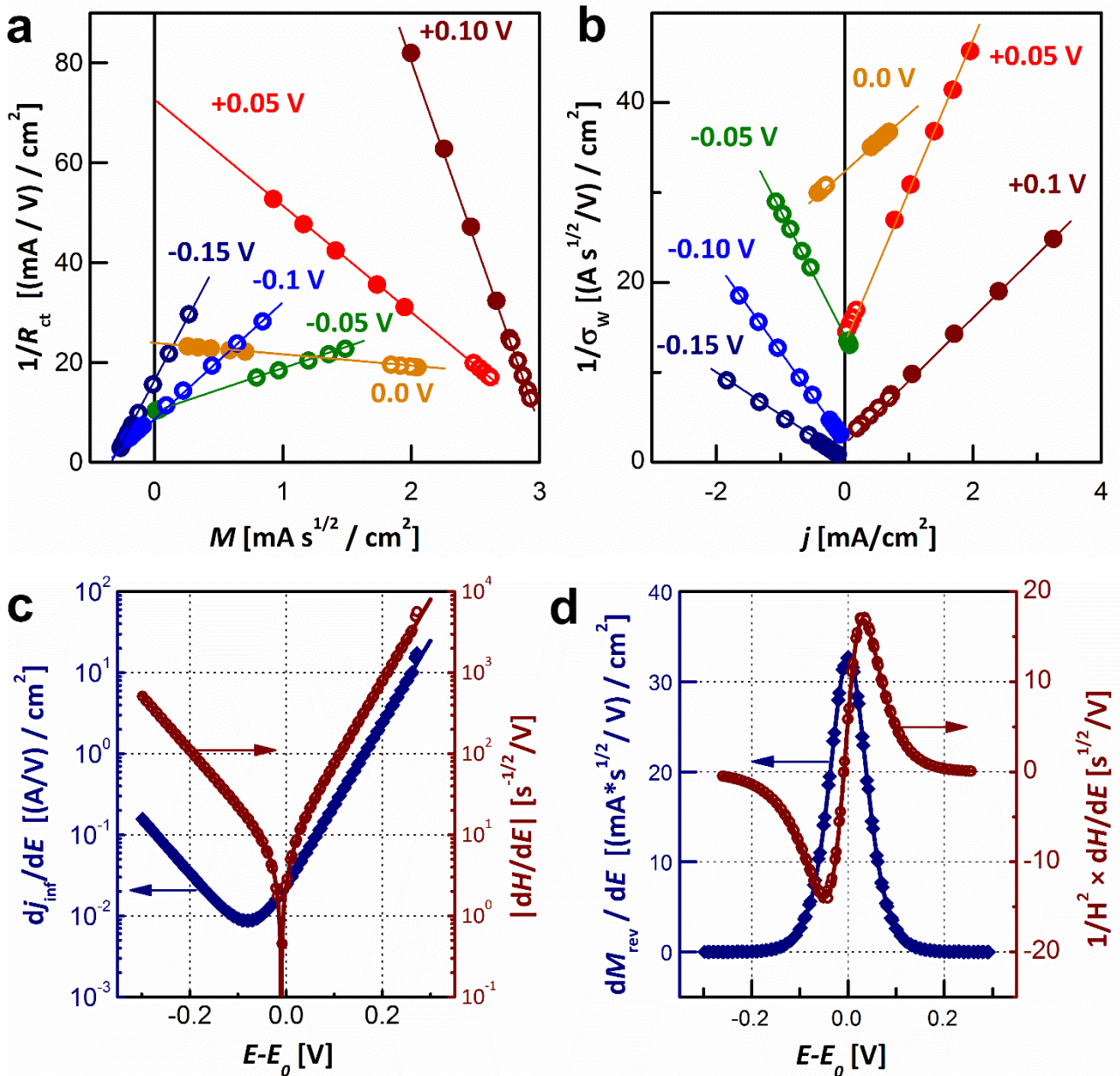
Fig.3. Demonstration of linearity (cf. Eqs. (11) and (17)) and of how the PPI functions are obtained from the intercepts and slopes.

a.) $1/R_{ct}$ vs M lines at potentials indicated. **b.)** $1/\sigma_W$ vs j lines at potentials indicated.

c.) Intercepts (blue diamonds) and slopes (red circles) of the $1/R_{ct}$ vs M lines of (**a**) as function of potential (cf. Eq. (11)). Solid lines: the input functions of dj_{inf}/dE and $|dH/dE|$ – same as those in Figs 1b and 1c.

d.) Intercepts (blue diamonds) and slopes (red circles) of the $1/\sigma_W$ vs j lines of (**b**) as function of potential (cf. Eq. (17)). Solid lines: the input functions of dM_{rev}/dE and $(1/H^2)\cdot dH/dE$ – same as those in Figs 1b and 1c.

3.3.   Tests of typical cases: numerical simulations (II)

The properties of the DEIS method have been demonstrated using an archetype of the quasi-reversible redox systems: the ferro-ferricyanide couple [4,7]. In these studies, however, no plots similar to Figs 2c and 2d have been created. The authors of these papers were aware of that the $R_{ct}(E)$ and $\sigma_W(E)$ functions should be different for the forward and backward scans – and both groups found very little differences. The simulations of this section may shed light on the reasons.

A simulation pair is shown with all parameters but the rate coefficients being the same. On Fig. 4a-4d CVs, $1/R_{ct}(E)$ and $1/\sigma_W(E)$ are shown, simulated for a redox couple with $k_0=10^{-3}$ cm/s, i.e. the same as at Fig 2. Note the increasing CV peak separation with scan-rate; the $1/R_{ct}(E)$ and $1/\sigma_W(E)$ functions have big hystereses. For the simulations of Fig 5a to 5c $k_0=10^{-2}$ cm/s was chosen – this is a k_0 value that is still an order of magnitude smaller than that of the ferro-ferricyanide couple [23]. For this latter system, the increase of the CV peak separation with scan-rate is barely visible, and the hystereses of the $1/R_{ct}(E)$ and $1/\sigma_W(E)$ functions almost vanish. To conclude, we can observe marked scan-rate dependences of the impedance-related parameters for those systems that exhibit a significant scan-rate dependence of the CV peak-separation.
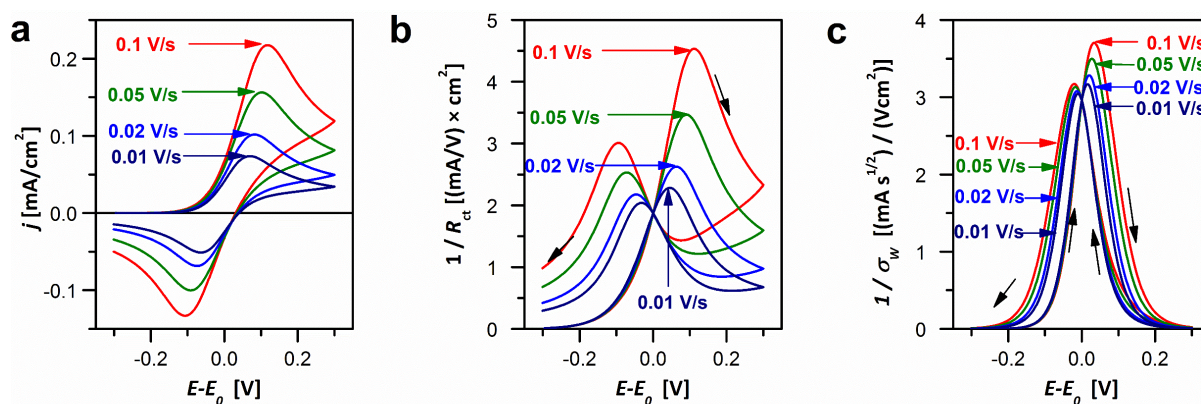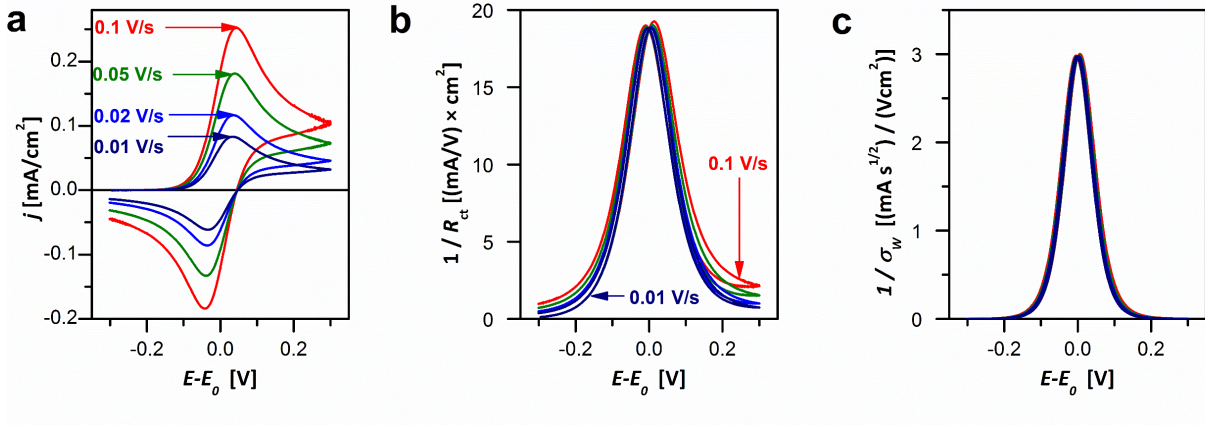

Fig.4. Simulated curves at scan-rates as indicated. **a.)** The CVs. **b.)** The $1/R_{ct}(E)$ functions. **c.)** The $1/\sigma_W(E)$ functions. The electrochemistry-related parameters of the simulation are as follows:

$c_{red}^b = 10^{-6}$ mol/cm^3, $c_{ox}^b = 0$ mol/cm^3, $D_{red} = D_{ox} = 10^{-5}$ cm^2/s;

$k_a(E) = k_0 \exp(\alpha_a F(E - E_0)/RT)$ and $k_c(E) = k_0 \exp(-\alpha_c F(E - E_0)/RT)$

with $k_0 = 10^{-3}$ cm/s; $\alpha_a = \alpha_c = 0.5$.

Fig. 5. Simulated curves at scan-rates as indicated. For details, see the legend of Fig.4. The only difference is $k_0 = 10^{-2}$ cm/s.

3.4. Transformation of AWVs to impedance spectrum parameters and back

Based on the above equations, we can transform voltammograms given as $j(E(t))$ and $H(E)$ function pairs (or any two of the j,H,M ensemble) to $R_{ct}(E)$ and $\sigma_W(E)$ pairs and back.

As an example we show how to transform voltammogram js and Ms to impedance parameters (provided that we know $H(E)$). We start with Eq. (13):

$$\frac{\mathrm{d}j}{\mathrm{d}E} = \frac{\mathrm{d}(j_{\mathrm{inf}} - H \cdot M)}{\mathrm{d}E} = \frac{1}{R_{\mathrm{ct,inf}}} - \frac{\mathrm{d}(H \cdot M)}{\mathrm{d}E} \tag{20}$$

By substituting $1/R_{\mathrm{ct,inf}}$ from Eq. (11), we get

$$\frac{1}{R_{\mathrm{ct}}} = \frac{\mathrm{d}j}{\mathrm{d}E} + H \cdot \frac{\mathrm{d}M}{\mathrm{d}E} = \frac{\mathrm{d}j}{\mathrm{d}E} + \frac{j_{\mathrm{inf}}}{M_{\mathrm{rev}}} \cdot \frac{\mathrm{d}M}{\mathrm{d}E} \tag{21}$$

With $\sigma_W = R_{\mathrm{ct}} \cdot H$ (cf. Eq.(5)) we get

$$\frac{1}{\sigma_W} = \frac{1}{H} \cdot \frac{\mathrm{d}j}{\mathrm{d}E} + \frac{\mathrm{d}M}{\mathrm{d}E} = \frac{M_{\mathrm{rev}}}{j_{\mathrm{inf}}} \cdot \frac{\mathrm{d}j}{\mathrm{d}E} + \frac{\mathrm{d}M}{\mathrm{d}E} \tag{22}$$

Note the simplicity and symmetry of Eqs. (21) and (22).

13

3.5. Summary of the important equations

	charge transfer	coupling	diffusion
CV	$j = j_{\mathrm{inf}} - H \cdot M$	$H = j_{\mathrm{inf}}/M_{\mathrm{rev}}$	$M = M_{\mathrm{rev}} - 1/H \cdot j$
DEIS	$\dfrac{1}{R_{\mathrm{ct}}} = \dfrac{\mathrm{d}j_{\mathrm{inf}}}{\mathrm{d}E} - \dfrac{\mathrm{d}H}{\mathrm{d}E} \cdot M$	$H = \sigma_{\mathrm{W}}/R_{\mathrm{ct}}$	$\dfrac{1}{\sigma_{\mathrm{W}}} = \dfrac{\mathrm{d}M_{\mathrm{rev}}}{\mathrm{d}E} + \dfrac{1}{H^2}\dfrac{\mathrm{d}H}{\mathrm{d}E} \cdot j$

Table 2. The relation of the four important equations connecting the four measured quantities $(j, M, R_{\mathrm{ct}}, \sigma_{\mathrm{W}})$ with the four PPI quantities $(j_{\mathrm{inf}}, M_{\mathrm{rev}}, \mathrm{d}j_{\mathrm{inf}}/\mathrm{d}E, \mathrm{d}M_{\mathrm{rev}}/\mathrm{d}E)$.

The important equations and their relations are summarized in Table 2. Two points need emphasis: (i) The CV and the DEIS measure the large and small signal ("global" and "local") responses of the system. The slopes and intercepts of the linear equations of the DEIS are just the potential derivatives of those of the CV equations. (ii) Note the central role of the parameter combination $H = k_{\mathrm{a}}/\sqrt{D_{\mathrm{red}}} + k_{\mathrm{c}}/\sqrt{D_{\mathrm{ox}}}$. in the equation set.

3.6. Practical implication: determination of the charge transfer rate coefficients

1. The determination of electrochemical charge transfer rates usually requires high purity experiments, because the measurement is very sensitive to the cleanliness of the interface. One may reduce the spoiling of the interface if the experiment is carried out quickly. This is the big advantage of DEIS, where a CV cycle along with one hundred audio-frequency impedance spectra can be acquired within less than a minute; meanwhile, in case of EIS, measurements may last for hours. The main role of the above derivation is that it clearly shows the connection of the $\sigma_{\mathrm{W,ss}}$, σ_{W}, $R_{\mathrm{ct,inf}}$ and R_{ct} parameters, and their roles in classical EIS and DEIS studies.

2. One cannot determine rate coefficients directly from voltammetry or impedance measurements. All what we can obtain is the $H(E)$ function of Eq. (5), which is a combination of rate coefficients and diffusion coefficients. Fortunately, the latter ones are independent of potential and can be obtained through special $M_{\mathrm{rev}}(|E \gg E_{1/2}|)$ measurements (like measuring Cottrell-transients). Even then, to separate the anodic and cathodic rate

coefficients, we have to assume a certain (typically exponential) potential dependence of them.

3. Determination of rate coefficients from CVs has two difficulties. The first is due to the non-zero electrolyte resistance, to the so-called "IR-drop". This can be significantly reduced by electronic IR-compensation or can be corrected by the procedure explained in Section 3.2.2. of [11]. The second difficulty is the consequence of that the double layer's charging current depends on many (often uncontrollable) parameters. The double layer capacitance, C_{dl}, – being the attribute of the interface – is very sensitive to contaminations of the solution and hence it is difficult to make any "double layer correction" or "baseline correction". That is why the evaluation is indefinite also with the traditional ways of CV evaluations listed in Section 3.2.4. of [11]. Using DEIS is a good alternative: by fitting an appropriate equivalent circuit (typically a Randles-circuit) the σ_W and R_{ct} quantities are separated from the obtained C_{dl} and R_s. (We note that in many cases C_{dl} is to be replaced by a constant-phase element to obtain a good fit, but this is a minor complication which has not much effect on the kinetics-related parameters much.)

4. For impedance measurements, we always assume the steady state of the system; in the present case, that of the overlined concentrations in Eq.3. Evidently, this condition holds for slow scans with high frequency impedance measurements and does not hold for fast scans with low frequencies. The maximum scan-rate depends on how fast we can measure the impedance spectra, which in turn, depends on many technical details of the impedance spectrum measurement. There exist no exact, unique equation relating the maximum scan-rate to the frequency range of impedance measurement; however, as a thumb's rule, we can say that the spectrum measurement is correct if the potential change during a spectrum measurement is smaller than RT/F ($\approx$27 mV). (Note that if a Kramers-Kronig test reveals non-self-consistency at the low frequency end of the spectrum, even then it is easy to truncate the impedance spectrum by discarding a couple of points of the lowermost frequencies.)
An example: in preliminary experiments of the present author, using a setup similar to the one described in Ref. 3, spectra comprising 41 spectrum points in the 10 Hz and 13.2 kHz frequency range could be measured in every 300 ms; during this time, with 50 mV/s scan-rate the potential changed 15 mV. Hence, for this particular measurement system with 10 Hz low frequency limit, the scan-rate was limited to 50 mV/s.

5. One role of this theory is to help to understand the origin of differences in the σ_W and R_{ct} parameters measured by EIS and DEIS. By EIS we determine $\sigma_{W,ss}$ (= $(dM_{rev}/dE)^{-1}$ cf. Eq. (19)) and $R_{ct,ss}$ (= $(H \cdot dM_{rev}/dE)^{-1}$, cf. Eq. (18)); their ratio is just the same H as of the σ_W and R_{ct} obtained from spectra acquired by DEIS.

4. Conclusions

The previous theory of Ref. [11] showed how to transform quasi-reversible voltammograms to yield two potential-program invariant functions, j_{inf} and M_{rev}. The present theory plays a similar role by producing two other potential-program invariant (e.g. scan-rate invariant) functions for the Faraday admittance, $R_{ct, inf}$ and $\sigma_{W, rev}$. j_{inf} and M_{rev} are the large signal response curves ("global" response functions) of the system whereas the reciprocals of $R_{ct, inf}$ and $\sigma_{W, rev}$ are the small signal, or "local" response functions. The local response functions are the potential derivatives of the global response functions. The connections between the measured and the PPI functions – as summarized in Table 2 – are surprisingly simple.

From the point of view of measurements of charge transfer kinetics, it is of great importance that the $H = \sigma_W/R_{ct}$ equation holds also for spectra measured by DEIS. This opens a new route for the high accuracy determination of charge transfer rate coefficients of quasi-reversibe redox systems.

Declarations of interest: none.

List of symbols

t, E, v	time, electrode potential, scan-rate
j, j_{inf}	current density, and current density at infinite transport
$R_{\text{ct}}, R_{\text{ct, inf}}$	charge transfer resistance and charge transfer resistance at infinite transport rate
$R_{\text{ct,ss}}$	charge transfer resistance in the steady state of the electrode
M, M_{rev}	semiintegrated current density (cf. Eq.(8)), and semiintegrated current density for reversible redox systems
$\sigma_{\text{W}}, \sigma_{\text{W, ss}},$	Warburg coefficient and Warburg coefficient in the steady state of the electrode; see also Section 3.1
$c_{\text{red}}, c_{\text{ox}}$	concentration of the reduced and oxidized species in the electrolyte bulk
$c_{\text{red}}^{\text{s}}, c_{\text{ox}}^{\text{s}}$	concentration of the reduced and oxidized species at the electrode surface
$D_{\text{red}}, D_{\text{ox}}$	diffusion coefficient of the reduced and oxidized species
$k_{\text{a}}, k_{\text{c}}$	rate coefficient of the anodic and cathodic reactions
$\alpha_{\text{a}}, \alpha_{\text{c}}$	charge transfer coefficient of the anodic and cathodic reactions
k_0, E_0	standard rate coefficient and standard potential of the redox reaction
H	parameter combination of $k_{\text{a}}, k_{\text{c}}, D_{\text{red}},$ and D_{ox} (cf. Eq.(5)).
n	charge number of the electrode reaction
F,R,T	Faraday's number, universal gas constant, temperature

Appendix A. The simulation algorithm

The core of the CV simulation algorithm, as a pseudocode is as follows. All the variable names are the same as those in the "Theory" section (though typographically different). The FRLT() function is the fast semiintegration algorithm ("Fast Riemann-Liouville-Transform algorithm"). In fact, it is a low-pass recursive filter array, constructed to have a transfer characteristics of $1/\sqrt{s}$ in the Laplace space. For details, including the initialization of the filter array, see Ref. 21.

```
do
        t(i)=t(i-1)+deltat
        E(i)=CalculateNextPotential_for_ t(i)
        ka(i) = k0 × Exp(+alphaa × FperRT * (E(i) - E0))
        kc(i) = k0 × Exp(-alphac × FperRT * (E(i) - E0))
        H(i)=ka(i)/sqrt(Dred)+ kc(i)/sqrt(Dox)          'cf. Eq. (5)
        j(i) = nF×ka(i)×csred – nF×kc(i)×csox           'cf. Eq. (1)
        M(i) = FRLT(j(i))
        csred = cbred – M(i) / (nF×SqrOfDred)           'cf. Eq (6)
        csox = cbox + M(i) / (nF×SqrOfDox)              'cf. Eq. (7)

        dE=E(i)-E(i-1)
        dka=ka(i)-ka(i-1)
        dkc=kc(i)-kc(i-1)
        Rct(i)=1/(nF×(csred×dka – csox×dkc/dE))         'cf. Eq.(3)
        sigmaW(i)=Rct(i)*H(i)                            'cf. Eq. (5)

        WriteDataToFile(t,E,j,M,Rct,sigmaW)

        jinf(i) = nF×ka(i)×cbred – nF×kc(i)×cbox        'cf. Eq. (2)
        Mrev(i)=jinf(i)/H(i)                             'cf. Eq. (15)
        WriteDataToFile(H, jinf, Mrev)
loop for all data
```

References:

1   S.C. Creason, D.E. Smith: Fourier transform Faradaic admittance measurements: I. Demonstration of the applicability of random and pseudo-random noise as applied potential signals, J. Electroanal. Chem. Interf. Electrochem., 36 (1972) A1.

2   J. Házi, D. M. Elton, W. A. Czerwinski, J. Schiewe, V. A. Vincente-Beckett, A. M. Bond, J. Electroanal. Chem., 499 (1997) 48

3   L. Sacci, D. A. Harrington, Dynamic Electrochemical Impedance Spectroscopy, ECS Transactions, 19 (2009) 31-42

4   G. A. Ragoisha, A. S. Bondarenko, Potentiodynamic electrochemical impedance spectroscopy, Electrochimica Acta, 50 (2005) 1553

5   K. Darowicki, P. Slepski, Dynamic electrochemical impedance spectroscopy of the first order electrode reaction, J. Electroanal. Chem., 547 (2003) 1

6   S.B. Emery, J.L. Hubbley, D. Roy, Time resolved impedance spectroscopy as a probe of electrochemical kinetics: The ferro/ferricyanide redox reaction in the presence of anion adsorption on thin film gold, Electrochim. Acta 50 (2005) 5659

7   D. Koster, G. Du, A. Battistel, F.La Mantia, Dynamic impedance spectroscopy using dynamic multi-frequency analysis: A theoretical and experimental investigation, Electrochim. Acta, 246 (2017) 553

8   A.S. Bandarenka, Exploring the interfaces between metal electrodes and aqueous electrolytes with electrochemical impedance spectroscopy, Analyst 138 (2013) 5540

9   A.J. Bard and L.R. Faulkner, Electrochemical Methods, 2nd ed. Wiley, 2001.

10   M. Sluyters-Rehbach, Impedances of electrochemical systems, Terminology, nomenclature and representation, Pure &Appl. Chem., 66 (1994) 1831.

11   T. Pajkossy, S. Vesztergom, Analysis of voltammograms of quasi-reversible redox systems: Transformation to potential program invariant form, Electrochim. Acta, 297 (2019) 1121.

12   J.E.B. Randles, Kinetics of rapid electrode reactions. Disc. Farad. Soc. 1 (1947) 11.

13   A. Lasia, Electrochemical Impedance Spectroscopy and its Applications, Springer, 2014,

14   R. de Levie, A.A. Husovsky, On the negative Faradaic admittance in the region of the polarographic minimum of In(III) in aqueous NaSCN solution, J. Electroanal. Chem., 22 (1969) 29

15   R. de Levie, L. Pospisil, On the coupling of interfacial and diffusional impedances, and on the equivalent circuit of an electrochemical cell, J. Electroanal. Chem. 22 (1969) 277.

16   H.Matsuda, Y.Ayabe, Zur Theorie der Randles-Sevčikschen Kathodenstrahl-Polarographie, Z. Elektrochemie 59 (1955) 494.

17   K.B. Oldham, A signal-independent electroanalytical method, Anal. Chem, 44 (1972) 196.

18   K.B. Oldham, J.C. Myland, A.M. Bond, Electrochemical science and technology: fundamentals and applications, Wiley, 2012, Ch.12.

19   T. Pajkossy, Potential program invariant representation of voltammetric measurement results of reversible redox couples, J. Electroanal. Chem. 422 (1997) 13.

20   S. Vesztergom, A short introduction to digital simulations in electrochemistry: Simulating the Cottrell experiment in NI LabVIEW, J. Electrochem. Sci. Eng. 8 (2018) 171.

21   T. Pajkossy, L. Nyikos, Fast algorithm for differintegration, J. Electroanal. Chem. 179 (1984) 65.

22   P.R. Bevington, D.K. Robinson, Data reduction and error analysis for the physical sciences, 3d ed. McGraw-Hill, 2003, Ch.6.

23   D.H. Angell, T. Dickinson, The kinetics of the ferrous /ferric and ferro/ferricyanide reactions at platinum and gold electrodes, J. Electroanal. Chem., 35 (1972) 55